

Active Deep Learning Guided by Efficient Gaussian Process Surrogates

Yunpyo An, Suyeong Park and Kwang In Kim*

UNIST

{anyunpyo, suyeong, kimki}@unist.ac.kr

Abstract

The success of active learning relies on the exploration of the underlying data-generating distributions, populating sparsely labeled data areas, and exploitation of the information about the task gained by the baseline (neural network) learners. In this paper, we present a new algorithm that combines these two active learning modes. Our algorithm adopts a Bayesian surrogate for the baseline learner, and it optimizes the exploration process by maximizing the gain of information caused by new labels. Further, by instantly updating the surrogate learner for each new data instance, our model can faithfully simulate and exploit the continuous learning behavior of the learner without having to actually retrain it per label. In experiments with four benchmark classification datasets, our method demonstrated significant performance gain over state-of-the-arts.

1 Introduction

The success of deep learning relies on the abundance of labeled data. However, constructing large-scale datasets can be challenging for problems that incur high labeling costs. The application of deep learning is therefore limited to areas where sufficient labeling budgets can be provided. Active learning aims to break this limitation by selecting the most *informative* data instances to label given fixed labeling budgets [Ren *et al.*, 2020; Settles, 2009; Aggarwal *et al.*, 2015]. Due to its capability to enhance the labeling efficiency, active learning has been widely used in data-sparse learning problems including medical imaging [Budd *et al.*, 2019; Kim *et al.*, 2020], image and video analysis [Yoo and Kweon, 2019; Sinha *et al.*, 2019; Abu-El-Haija *et al.*, 2016], ranking [Ailon, 2012; Donmez and Carbonell, 2009], bio- and health informatics [Angeli *et al.*, 2021; Mohamed *et al.*, 2010], and natural language processing [Siddhant and Lipton, 2018; Tomanek and Hahn, 2009].

Typically in active learning, the baseline learner is initially presented with a dataset where only a small subset is labeled.

During the learning process, active learning algorithms analyze the distribution of the data and progress achieved by the learner and based on that suggest unlabeled data instances to label. For this, most existing active learning approaches exercise *exploration* and/or *exploitation* [Bondu *et al.*, 2010]. Exploration aims to capture the global shape of the underlying data generation process and focuses on populating the areas where the labels are sparsely sampled. This process is especially effective at the early stages of learning (i.e. when the number of labels is small). However, its main limitation is that this process is by itself agnostic to the progress achieved by the learner. As more labels are acquired, the learner will become a more reliable estimator of the underlying ground truth. In this case, it might be more beneficial to focus on the areas where the learner struggles than trying to cover the areas where the learner is already confident even though no labels are sampled therein.

Exploitation (also known as *refinement*) addresses this limitation by identifying data where the predictions provided by the learner require deeper investigation. It selects instances on which the learner’s predictions are the most *uncertain*. However, at early learning stages, the learner might not have a good understanding of the problem, and the corresponding uncertainty estimates might be unreliable. Therefore, this process can be more effective in the later learning stages.

A significant challenge in exploration is identifying an optimal coverage of the data-generating process. Existing work approached this by formulating it into mathematically rigorous but complex combinatorial optimization problems [Sener and Savarese, 2018] or employing computationally efficient but less rigorous (and perhaps sub-optimal) methods, e.g. pre-clustering [Bodó *et al.*, 2011; Smeulder, 2004]. For exploitation, the main challenge is *continuously capturing* the learner’s progress as labels are added: As training neural networks is computationally demanding, updating the baseline model per new data instance is infeasible. On the other hand, naively selecting multiple uncertain (to predict) points at once might lead to spatial aggregations of points. If the learner prediction of a single data instance is uncertain, likely, its neighbors are also uncertain. However, labeling only one or few data instances will often be sufficient to resolve the uncertainties within this spatial aggregation. To address this, existing approaches employed additional data diversification processes [Smeulder, 2004; Sinha *et al.*, 2019].

*The first two authors contributed equally.

In this paper, we present a new active learning algorithm that combines exploration and exploitation based on a single surrogate to the neural network learner. Our algorithm uses a Gaussian process (GP) learner which is *continuously updated* (i.e. updated each time a single label is added) simulating the learning progress achieved by the neural learner.

Our approach offers unique advantages in both exploration and exploitation: 1) By adopting well-established Bayesian approaches, it offers computationally efficient and optimal exploration. At each stage, a new data instance is selected to maximize the resulting information gain on the *entire dataset*; 2) For exploitation, our model can quickly identify the most uncertain data points, and it *instantly* updates the surrogate GP learner: Once this learner is updated based on a newly added data point, the confidence of predictions on its spatial neighbors are immediately improved. There is no need to employ additional data diversification models.

In the experiments with four datasets, our algorithm was significantly better than or comparable to state-of-the-art approaches at early, as well as later stages of learning.

2 Related work

Existing active learning approaches can be categorized into exploration-based approaches [Sener and Savarese, 2018; Aodha *et al.*, 2014; Smeulder, 2004], exploitation-based approaches [Yoo and Kweon, 2019; Tong and Koller, 2001; Yun *et al.*, 2020; Kirsch *et al.*, 2019], and their combinations [Ash *et al.*, 2020; Elhamifar *et al.*, 2013]. Exploration-based approaches focus on efficiently covering the underlying data-generating distribution. This can be achieved by performing pre-clustering of unlabeled data [Smeulder, 2004], predicting how the predictions would change if the individual data instances are labeled [Aodha *et al.*, 2014], or maximizing the mutual information between labeled and unlabeled data instances [Guo, 2010], all helping diversify selected labels. Sener and Savarese’s core-set approach minimizes an upper bound on the generalization error, leading to minimum coverings of data space via labeled data [Sener and Savarese, 2018]. [Geifman and El-Yaniv, 2017] employed a similar idea instantiated as a sequential algorithm that selects farthest traversals from the labeled data instances. [Gissin and Shalev-Shwartz, 2019] also fd the diversity by selecting data points in the way that the labeled points and the unlabeled points become indistinguishable. [Sinha *et al.*, 2019]’s variational adversarial active learning (VAAL) achieved sample diversity by constructing a latent space using a variational autoencoder and an adversarial network that distinguishes labeled and unlabeled data. Exploration-based approaches are effective in selecting the most representative data points, but they are limited in that the information of the learning task acquired by the baseline learner is not fully exploited.

Exploitation-based approaches identify the areas where the learner’s predictions are uncertain. [Tong and Koller, 2001]’s approach selects data instances that are close to the decision boundary of the support vector machine learner. Selecting data instances that maximize the entropy of the predictive class-conditional distribution is also commonly exercised [Yun *et al.*, 2020]. For Bayesian learners, [Houlsby

et al., 2011]’s Bayesian active learning by disagreement (BALD) algorithm selects data by maximizing the information gain. [Kirsch *et al.*, 2019] extended this approach to deep learning by simultaneously suggesting multiple instances for labeling (BatchBALD). [Tran *et al.*, 2019] further extended BALD by combining it with generative models such that informative data instances are synthesized instead of being selected from the data pool. [Yoo and Kweon, 2019]’s learning loss algorithm trains a separate module that predicts the losses of the learner and selects data instances that incur the highest predicted losses. Exploitation-based approaches are especially powerful when the learner’s predictions faithfully approximate the underlying ground truth. However, at early learning stages, the learners’ predictions are unreliable, and the corresponding active learning performance can degrade.

[Elhamifar *et al.*, 2013] combined exploration and exploitation by integrating the diversity of labels and learner’s predictive uncertainty into a convex optimization problem. [Zhang *et al.*, 2020]’s state-relabeling adversarial active learning (SRAAL) extends VAAL to accommodate model uncertainty. This algorithm is tailored for specific types of learners that share their latent space with variational autoencoders. [Ash *et al.*, 2020]’s batch active learning by diverse gradient embeddings (BADGE) also trades diversity and uncertainty by analyzing the magnitude of the loss gradients of candidate points and their distances to previously labeled points. [Kim *et al.*, 2021]’s task-aware VAAL (TA-VAAL) extends VAAL to take into account the predicted learner losses. [Caramalau *et al.*, 2021]’s sequential graph convolutional network (GCN)-based algorithm improves uncertainty sampling via analyzing the overall distribution of data based on graph embeddings of data instances. In the experiments, we demonstrate that our method significantly outperforms or is on par with the state-of-the-art BADGE, TA-VAAL, and sequential GCN algorithms.

3 Active learning guided by Gaussian process surrogate learners

Suppose that we are given data spaces of inputs \mathcal{X} and outputs \mathcal{Y} . In the standard supervised learning, one learns a function $f : \mathcal{X} \rightarrow \mathcal{Y}$ based on a labeled training set $T = \{(\mathbf{x}_1, \mathbf{y}_1), \dots, (\mathbf{x}_N, \mathbf{y}_N)\} \subset \mathcal{X} \times \mathcal{Y}$ sampled from the joint distribution of \mathcal{X} and \mathcal{Y} . Instead, in active learning, initially only an input dataset $X = \{\mathbf{x}_1, \dots, \mathbf{x}_N\}$ is presented. The learning algorithm is then provided with a budget to suggest B data instances to label. The output of active learning is a labeled index subset L of $\{1, \dots, N\}$ of size B specifying the selected elements in T . We will focus on classification problems, and assume that our data are one-hot encoded such that $\mathcal{Y} \subset \mathbb{R}^C$ with C being the number of classes and the baseline learner f generates probabilistic outputs, i.e. $\|f(\mathbf{x})\|_1 = 1$ and $[f(\mathbf{x})]_j \geq 0$ with $[f(\mathbf{x})]_j$ being the j -th element (corresponding to the j -th class) of $f(\mathbf{x})$. With a slight abuse of notation, we will use f to denote both the baseline learning algorithm and its output (a classification function).

We take an incremental approach to build L . Starting from an initial index set of labeled points L^0 , at each stage t , L^t is augmented by a single label index l^t : $L^{t+1} =$

$L^t \cup \{l^t\}$. This process is facilitated by a *utility* function $u : \{1, \dots, N\} \rightarrow \mathbb{R}$ such that l^t is selected as the maximizer of u from $\{1, \dots, N\} \setminus L^t$.

A good utility function should capture 1) how difficult (or *uncertain*) each data instance is to make a classification decision and 2) how *influential* a data instance is to others when labeled, i.e. when a point is labeled, how the decisions for other instances are improved. Realizing these objectives requires the capability of *continuously observing* how f is updated per stage (f^t denotes the learner trained on L^t); Simultaneously selecting B data instances at a single stage as the first B maximizers of u will be sub-optimal considering that if a data instance \mathbf{x}_i has the highest utility $u(i)$, then it is likely that its spatial neighbors exhibit similarly high utility values. However, labeling such spatial aggregations can be redundant as once \mathbf{x}_i is labeled and f is accordingly retrained, then it will provide more accurate predictions on these neighbors. It is challenging to apply this continuous retraining strategy when f is deep neural networks (DNNs) due to prohibitively high computational costs. Existing approaches bypass this challenge by either designing a utility that is independent of the learner f (i.e. pure exploration) [Sener and Savarese, 2018; Aodha *et al.*, 2014; Smeulder, 2004] or by adopting auxiliary processes that promote spatial diversity of labeled data [Kirsch *et al.*, 2019; Smeulder, 2004; Sinha *et al.*, 2019]. The latter often requires tuning hyperparameters and/or heuristics to trade off the selection of difficult labels against retaining diversity.

Our approach is to learn a computationally efficient surrogate learner \hat{f} in parallel, simulating the continuous learning behavior of the baseline learner f . We use a Gaussian process (GP) estimator. This enables the use of well-developed Bayesian inference techniques in designing and efficiently evaluating the utility u . Furthermore, our approach does not require additional mechanisms to promote label diversity since when a data instance (with high utility) is labeled, the surrogate learner \hat{f} is instantly updated and the utilities of its neighbors are accordingly suppressed.

Gaussian process surrogate learner: For a given budget B , the DNN learner f is trained only at every I -th stage. The behavior of f in-between these I -th stages is captured by a surrogate GP learner \hat{f} that is continuously updated (retrained for each new label): At each I -th stage, our surrogate \hat{f} is given as f (we take softmax for the output layer). In between these I -th stages, \hat{f} is trained based on the difference between the surrogate at the I -th stages and the corresponding ground truth. For each new data instance \mathbf{x} selected for labeling, the corresponding GP training label is obtained as $\mathbf{y} - f(\mathbf{x})$. We will use two types of utility functions respectively representing how uncertain and influential the predictions made by f (and \hat{f}) are.

Suppose that t data instances are already labeled at stage t . Without loss of generality we will assume that these labeled points correspond to the first t points in X : $T^t = \{(\mathbf{x}_i, \mathbf{y}_i)\}_{i=1}^t$ constitutes a labeled training set while $U^t = \{\mathbf{x}_i\}_{i=t+1}^N$ serves as an unlabeled set, i.e. $L^t = \{1, \dots, t\}$.

Kernels: Our GP prior is instantiated based on a combina-

tion of Gaussian kernels constructed based on the inputs \mathbf{x} and \mathbf{x}' , and the corresponding outputs of the latest learner $f(\mathbf{x})$ and $f(\mathbf{x}')$:¹

$$k(\mathbf{x}, \mathbf{x}', f(\mathbf{x}), f(\mathbf{x}')) = k_{\mathbf{x}}(\mathbf{x}, \mathbf{x}')k_f(f(\mathbf{x}), f(\mathbf{x}')), \quad (1)$$

$$k_{\mathbf{x}}(\mathbf{x}, \mathbf{x}') = \exp\left(-\frac{\|\mathbf{x} - \mathbf{x}'\|^2}{\sigma_{\mathbf{x}}^2}\right), \quad (2)$$

$$k_f(\mathbf{y}, \mathbf{y}') = \exp\left(-\frac{\|\mathbf{y} - \mathbf{y}'\|^2}{\sigma_f^2}\right), \quad (3)$$

where $\sigma_{\mathbf{x}}^2, \sigma_f^2 > 0$ are hyperparameters. Using this product kernel helps the resulting surrogate \hat{f} faithfully capture the behavior of the underlying deep learner f and enables us to avoid smoothing over the class boundaries formed f . When we train a separate baseline network at an intermediate stage of 4,500 labels (for the CIFAR10 dataset; see Sec. 4 for details), experiments on 10 different random initializations showed that the mean absolute deviation between \hat{f} and f on a training set was reduced by 42% (at around 0.012) from the case of using only the standard kernel $k_{\mathbf{x}}$.

Predictive model: Our GP learner \hat{f} uses an i.i.d. Gaussian likelihood across all classes and data instances [Rasmussen and Williams, 2006]: $[\mathbf{y}]_j \sim \mathcal{N}([f(\mathbf{x})]_j, \sigma^2)$ with $\mathcal{N}(\mu, \sigma^2)$ being the Gaussian distribution with mean μ and variance σ^2 . Combining this likelihood with the GP prior (Eq. 1), the prediction of \hat{f} for an unlabeled point $\mathbf{x}_i \in U^t$ is given as a Gaussian random vector of size C :

$$p(\mathbf{y}_i | T^t, \mathbf{x}_i) = \mathcal{N}(\boldsymbol{\mu}_i^t, \boldsymbol{\Sigma}_i^t), \text{ where} \quad (4)$$

$$\boldsymbol{\mu}_i^t = (\mathbf{k}_i^t)^\top (\mathbf{K}^t + \sigma^2 \mathbf{I})^{-1} \mathbf{Y}^t,$$

$$\boldsymbol{\Sigma}_i^t = (1 - (\mathbf{k}_i^t)^\top (\mathbf{K}^t + \sigma^2 \mathbf{I})^{-1} \mathbf{k}_i^t) \mathbf{I},$$

$\mathbf{k}_i^t = [k(\mathbf{x}_i, \mathbf{x}_1, f(\mathbf{x}_i), f(\mathbf{x}_1)), \dots, k(\mathbf{x}_i, \mathbf{x}_t, f(\mathbf{x}_i), f(\mathbf{x}_t))]^\top$, $[\mathbf{K}^t]_{mn} = k(\mathbf{x}_m, \mathbf{x}_n, f(\mathbf{x}_m), f(\mathbf{x}_n))$ for $1 \leq m, n \leq t$, and $\mathbf{Y}^t = [\mathbf{y}_1^\top, \dots, \mathbf{y}_t^\top]^\top$. This model requires inverting the kernel matrix \mathbf{K}^t of size $t \times t$ which grows quickly as active learning progresses. To maintain the computational complexity of \hat{f} -predictions (Eq. 4) at a manageable level, we adopt a sparse GP approximation [Snelson and Ghahramani, 2006] using two sets of basis points $U = \{\mathbf{u}_1, \dots, \mathbf{u}_K\}$ and $V = \{\mathbf{v}_1, \dots, \mathbf{v}_K\}$:

$$\boldsymbol{\mu}_i^t \approx (\mathbf{k}_i^t)^\top (\mathbf{Q}^t)^{-1} \mathbf{K}_{XP}^t (\boldsymbol{\Lambda}^t + \sigma^2 \mathbf{I})^{-1} \mathbf{Y}^t, \quad (5)$$

$$\boldsymbol{\Sigma}_i^t \approx (1 - (\mathbf{k}_i^t)^\top (\mathbf{K}_{PP}^{-1} - (\mathbf{Q}^t)^{-1}) \mathbf{k}_i^t) \mathbf{I} + \sigma^2 \mathbf{I}, \text{ where}$$

$$\mathbf{Q}^t = \mathbf{K}_{PP} + (\mathbf{K}_{XP}^t)^\top (\boldsymbol{\Lambda}^t + \sigma^2 \mathbf{I})^{-1} \mathbf{K}_{XP}^t,$$

$\mathbf{k}_i^t = [k(\mathbf{x}_i, \mathbf{u}_1, f(\mathbf{x}_i), \mathbf{v}_1), \dots, k(\mathbf{x}_i, \mathbf{u}_K, f(\mathbf{x}_i), \mathbf{v}_K)]^\top$, for $1 \leq m \leq t$, $[\mathbf{K}_{XP}^t]_{mn} = k(\mathbf{x}_m, \mathbf{u}_n, f(\mathbf{x}_m), \mathbf{v}_n)$, $[\mathbf{K}_{PP}]_{mn} = k(\mathbf{u}_m, \mathbf{u}_n, \mathbf{v}_m, \mathbf{v}_n)$, and $\boldsymbol{\Lambda}^t$ is a diagonal matrix with its n -th entry $[\boldsymbol{\Lambda}^t]_{nn}$ defined as $1 - (\mathbf{k}_n^t)^\top \mathbf{K}_{PP}^{-1} \mathbf{k}_n^t$. The basis points U are obtained as the cluster centers of X

¹To calculate the output kernel k_f values, the learner values $\{f(\mathbf{x}_i)\}$ are stored at the beginning of each training interval (of size I); See Algorithm 1 and Sec. 4.

found using K -means clustering while V are randomly sampled as C -dimensional probability simplexes. The computational complexity of evaluating a prediction (Eq. 5) now becomes linear with respect to labeled data points: $\mathcal{O}(tK^2)$.

Predictive variance-based utility u^1 : As a Bayesian model, the output of \hat{f} for an unlabeled input \mathbf{x}_i is a probability distribution $p(\mathbf{y}_i|T^t, \mathbf{x}_i)$ providing a natural way of quantifying the uncertainty. The j -th diagonal element of the predictive covariance matrix for an input \mathbf{x}_i represents the entropy of the prediction about j -th class.² The trace of this matrix then captures overall, how uncertain the current model prediction is about \mathbf{x}_i . The entropies of individual data points by themselves do not reflect how *influential* these entities are when labeled, and therefore, naively maximizing this term tends to select outliers. This can be seen by the fact that the (diagonal terms of) predictive covariance Σ_i^t tends to increase as the corresponding unlabeled points deviate from the labeled training set; See [Sollich and Williams, 2005] for an analysis of this behavior for large-scale problems. Instead, we define the utility $u^1(i)$ based on how the predictive entropies of the *entire remaining unlabeled set* U^{t-1} are reduced once \mathbf{x}_i is labeled. For this, we keep the predictive covariance of the unlabeled set at each consecutive stage. Since covariance estimates are isotropic in our model, we store only a single diagonal entry per data point:

$$\begin{aligned} u^1(i) &= \sum_{j=t+1}^N \text{trace}[\Sigma_j^t] - \sum_{j=t+1}^N \text{trace}[\Sigma_j(i)] \quad (6) \\ &= C \sum_{j=t+1}^N (\mathbf{k}_j^t)^\top (\mathbf{Q}(i)^{-1} - (\mathbf{Q}^t)^{-1}) \mathbf{k}_j^t, \end{aligned}$$

where $\Sigma_j(i)$ denotes the covariance for $\mathbf{x}_j \in U^{t-1} \setminus \{\mathbf{x}_i\}$ predicted by the model trained on T^t and \mathbf{x}_i (assuming that \mathbf{x}_i is labeled),

$$\begin{aligned} \mathbf{Q}(i) &= \mathbf{K}_{PP} + \quad (7) \\ &\begin{pmatrix} \mathbf{K}_{XP}^t \\ (\mathbf{k}_i^t)^\top \end{pmatrix}^\top \left(\begin{pmatrix} \mathbf{\Lambda}^t & 0 \\ 0 & \lambda_i \end{pmatrix} + \sigma^2 \mathbf{I} \right)^{-1} \begin{pmatrix} \mathbf{K}_{XP}^t \\ (\mathbf{k}_i^t)^\top \end{pmatrix}, \end{aligned}$$

and $\lambda_i = 1 - (\mathbf{k}_i^t)^\top \mathbf{K}_{PP}^{-1} \mathbf{k}_i^t$. Directly calculating $u(i)$ takes $\mathcal{O}(tK^2 + K^3)$ -time which is prohibitive even for moderately-sized datasets. A computationally efficient solution is obtained by noting that the difference between $\mathbf{Q}(i)$ and \mathbf{Q}^t is rank one in that

$$\mathbf{Q}(i) = \mathbf{Q}^t + \mathbf{a}\mathbf{a}^\top \text{ with } \mathbf{a} = \frac{\mathbf{k}_i^t}{\sqrt{\lambda_i + \sigma^2}}. \quad (8)$$

Applying the *Sherman–Morrison–Woodbury* matrix identity [Schott, 2016] to Eq. 7 using Eq. 8, we obtain

$$u^1(i) = C \sum_{j=t+1}^N (\mathbf{k}_j^t)^\top \left(\frac{(\mathbf{Q}^t)^{-1} \mathbf{k}_i^t (\mathbf{k}_i^t)^\top (\mathbf{Q}^t)^{-1}}{\lambda_i + \sigma^2 + (\mathbf{k}_i^t)^\top (\mathbf{Q}^t)^{-1} \mathbf{k}_i^t} \right) \mathbf{k}_j^t.$$

With this form, the utility $u^1(i)$ can be evaluated in $\mathcal{O}(K^2)$ -time when $(\mathbf{Q}^t)^{-1}$ is provided. Once the inverse $(\mathbf{Q}^0)^{-1}$ is

²The variance of a Gaussian distribution is proportional to its entropy.

explicitly calculated at stage 0, at each stage t , $(\mathbf{Q}^t)^{-1}$ can also be calculated based on $(\mathbf{Q}^{t-1})^{-1}$ in $\mathcal{O}(K^2)$ -time.

Discussion: Our approach is inspired by Bayesian active learning approaches that minimize the entropy of the learner f parameters and their approximations (e.g. [Houlsby *et al.*, 2011; Kirsch *et al.*, 2019]). However, unlike these approaches, we minimize the entropy over the predictions made on the *entire data*. This makes our entropy calculation independent of the parametric forms of f and enables to use GP as a surrogate of a deep learner f .

Using the utility function u^1 , our model determines the next label l^t as the maximizer of u^1 over the unlabeled data index set $\{t+1, \dots, N\}$. This approach is feasible as u^1 does not require the actual label of a candidate point \mathbf{x}_i even though u^1 was derived based on the assumption that \mathbf{x}_i is labeled. This property stems from the i.i.d. Gaussian noise model. In general, for an underlying classification function \tilde{f} , the likelihood $p(\mathbf{y}|\tilde{f}(\mathbf{x}))$ of observing data \mathbf{y} given an input \mathbf{x} is not Gaussian and for that, logistic likelihood models are more commonly used in GP models. However, these lead to covariance predictions that explicitly involve the label of each candidate, but such labels become available only when the corresponding data points are actually selected.

Class-conditional entropy-based utility u^2 : This is based on the entropies of the class-conditional predictive distributions made by DNNs; applying the softmax activation, the final DNN output $f(\mathbf{x}_i)$ for an input \mathbf{x}_i is given as a probability distribution of size C on which the entropy can be measured. This differs from the entropy used in u^1 which is defined for continuous GP predictive distributions. A straightforward way to design u^2 is to measure the entropy of f -prediction at each stage:

$$\hat{u}^2(i) = \text{Ent}(f^t(\mathbf{x}_i)) \quad (9)$$

with $\text{Ent}(\mathbf{p})$ being the entropy of a distribution \mathbf{p} .

Maximizing $\hat{u}^2(i)$ can effectively select the most uncertain point to classify. However, implementing this strategy requires retraining f^t at each stage which is infeasible due to the high training cost. Instead, we train f only at every I -th stage and use the GP surrogate to estimate the entropy values for the intermediate stages. Suppose that at stage s (at an integer multiple of I), the DNN classifier f^s is newly trained, and the corresponding entropy values $\{\text{Ent}(f^s(\mathbf{x}_{t+1})), \dots, \text{Ent}(f^s(\mathbf{x}_N))\}$ are calculated. The entropy values at intermediate stages are generated by calibrating the original DNN entropy values $\{\text{Ent}(f^s(\mathbf{x}_i))\}$ using the surrogate predictions. After initializing the calibrated entropy $\tilde{\text{Ent}}^s(f(\mathbf{x}_i))$ at stage s as $\text{Ent}(f^s(\mathbf{x}_i))$, the new entropy at stage $t > s$ is given as

$$u^2(i) = \tilde{\text{Ent}}^t(f(\mathbf{x}_i)) = \tilde{\text{Ent}}^{t-1}(f(\mathbf{x}_i)) \frac{\text{Ent}(\rho(\hat{f}^t(\mathbf{x}_i)))}{\text{Ent}(\rho(\hat{f}^{t-1}(\mathbf{x}_i)))},$$

where $\rho(\hat{f}^t(\mathbf{x}_i))$ is the softmax output of the mean prediction μ_i^t made by the GP surrogate \hat{f}^t . Annotating a data instance \mathbf{x}_i will reduce the uncertainty of GP predictions not only at \mathbf{x}_i but also at its neighbors. In this way, the calibrated entropies

reflect the continuous reduction of uncertainties caused by new labeled points during the intermediate stages.

Discussion: Our utility u^2 is defined based on the entropies of the class-conditional predictive distributions made by the baseline learner: Our algorithm selects data on which the (estimated) entropies are highest. We also explored the possibility of defining a utility u^3 based on how the predictive entropies of *all data instances* in the unlabeled set are reduced when a candidate point \mathbf{x}_i is labeled. As this quantity involves the label of each candidate \mathbf{x}_i , it cannot be directly evaluated. Instead, for each class $j \in \{1, \dots, C\}$, we tentatively assigned the corresponding class label to \mathbf{x}_i and measured the resulting entropy reduction. The final utility $u^3(i)$ was obtained as the average of these hypothetical entropy values weighted by the corresponding class probabilities $\{[f(\mathbf{x}_i)]_j\}$ predicted by the learner. In our preliminary experiments, the final classification accuracy achieved by our original utility u^2 was lower by only 0.2% on average than u^3 (on CIFAR10 dataset) while it was around 40 times faster than u^3 . The main bottleneck of u^3 evaluation was the computation of entropy values for the entire unlabeled set per hypothesized candidate. This competitive performance of u^2 can be attributed to the fact that, maximizing u^2 does not select outliers unlike the predictive entropies used in u^1 : When monotonically increasing activations (e.g. sigmoid and ReLU) are used, the DNN predictions tend to be over-confident on outliers (the points that deviate from the training set). While this artifact is not desirable for the purpose of classification in general, it has a favorable side-effect in active learning since outliers are not selected as they are assigned with low class-conditional entropy values.

Our utility u^1 uses the expected reduction of predictive variances when labeled. Theoretically, a more appealing approach might be to use the expected reduction of test errors. However, since ground-truth labels are not available, such error reduction cannot be directly calculated. Existing approaches therefore introduced certain model assumptions [Freytag *et al.*, 2014; Vijayanarasimhan and Kapoor, 2010] (which might hold for only specific learners) or used the learner predictions as surrogates to the underlying ground-truth [Roy and McCallum, 2001], similarly to our u^2 utility.

Trading exploration and exploitation: Our two utility functions u^1 and u^2 have complementary strengths: u^1 measures the overall reduction of uncertainty across the entire unlabeled set. This is especially suitable at the early stages of learning (i.e. the number of labels t is limited) but is limited in that it is agnostic to the task at hand; The predictive covariance Σ_i^t is entirely determined based on how the input data instances in X are distributed, and it is independent of the labels acquired (Eq. 5). On the other hand, u^2 exploits the label information captured by the entropy of $f(\mathbf{x})$. However, at early learning stages, the performance of the learner f would be limited, and therefore the estimated entropies can be unreliable.

We combine the strengths of u^1 and u^2 by automatically selecting one at each stage. At each stage t , u^1 or u^2 is selected based on comparing the *testing accuracy* increases S^t

Algorithm 1 Active learning guided by GP surrogates.

Input: Input data X , budget B , training interval I , threshold \mathcal{T} , and initial label set L^0

Output: Label index set L^B

```

1: for  $t = 1, \dots, 100$  do
2:   Calculate GP predictions and update  $\mathbf{Q}^t$  (Eq. 5);
3:    $l^t = \arg \max u^1$ ;
4:    $L^t = L^{t-1} \cup \{l^t\}$ ;
5: end for
6: Calculate the average accuracy increases  $S^0$ ;
7: for  $t = 101, \dots, B$  do
8:   Calculate GP predictions and update  $\mathbf{Q}^t$  (Eq. 5);
9:   if  $\text{mod}(t, I) = 0$  then
10:    Train  $f^t$ , and calculate  $\{\text{Ent}(\rho(f^t(\mathbf{x}_i)))\}$  and  $\{k_f(f^t(\mathbf{x}_i), \mathbf{v}_j)\}$  (Eq. 1);
11:   end if
12:   Calculate the average accuracy increases  $S^t$ ;
13:   if  $\frac{S^0}{S^t} < \mathcal{T}$  then
14:      $l^t = \arg \max u^1$ ;
15:   else
16:      $l^t = \arg \max u^2$ ;
17:   end if
18:    $L^t = L^{t-1} \cup \{l^t\}$ ;
19: end for
```

averaged over the time window of $[t - 100, t]$ with the initial value S^0 : u^1 is selected when $\frac{S^0}{S^t} < \mathcal{T}$ with a hyperparameter \mathcal{T} . Otherwise, u^2 is selected. As test data is not available, we instead take the newly labeled training data point at t , as a single test point before it is added to L^{t-1} . Since S^t is not defined when $t < 100$ we use u^1 for the first 100 stages.

Figure 1 illustrates the labeling behavior of our algorithm using a toy example: At early learning stages, our algorithm tended to select u^1 utility focusing on populating sparsely labeled data areas. As more labels are acquired, the (simulated) test accuracies of the baseline learner improved, and our algorithm accordingly selected u^2 focusing on more difficult labels. Algorithm 1 summarizes the proposed algorithm.

Approximation quality of the GP surrogates: By construction, our GP surrogate \hat{f} is the same as f at every I -th stage, and in-between these stages, \hat{f} can deviate from f . Empirically, we observed that \hat{f} faithfully captures the behavior of f thanks to the product kernel k (Eq. 1): When a separate neural network learner f' was trained at the intermediate stage of 2,500 labels (for FashionMNIST), the signal-to-noise ratio of \hat{f} from f' (at $t=2,500$) was 15.49dB. This noise level is comparable to the deviations from f' caused by retraining the DNN learners with the same training data but with random initializations.

Hyperparameters and time complexity: Our algorithm has four hyperparameters. The threshold \mathcal{T} for selecting modes of exploration (u^1) and exploitation (u^2) is fixed at 1.5. The number of basis points K for U , and V (Eq. 5) is determined by trading the computational complexity of GP predictions off with their approximation accuracies, and it is fixed at 500. The input kernel parameter $\sigma_{\mathbf{x}}$ is determined at

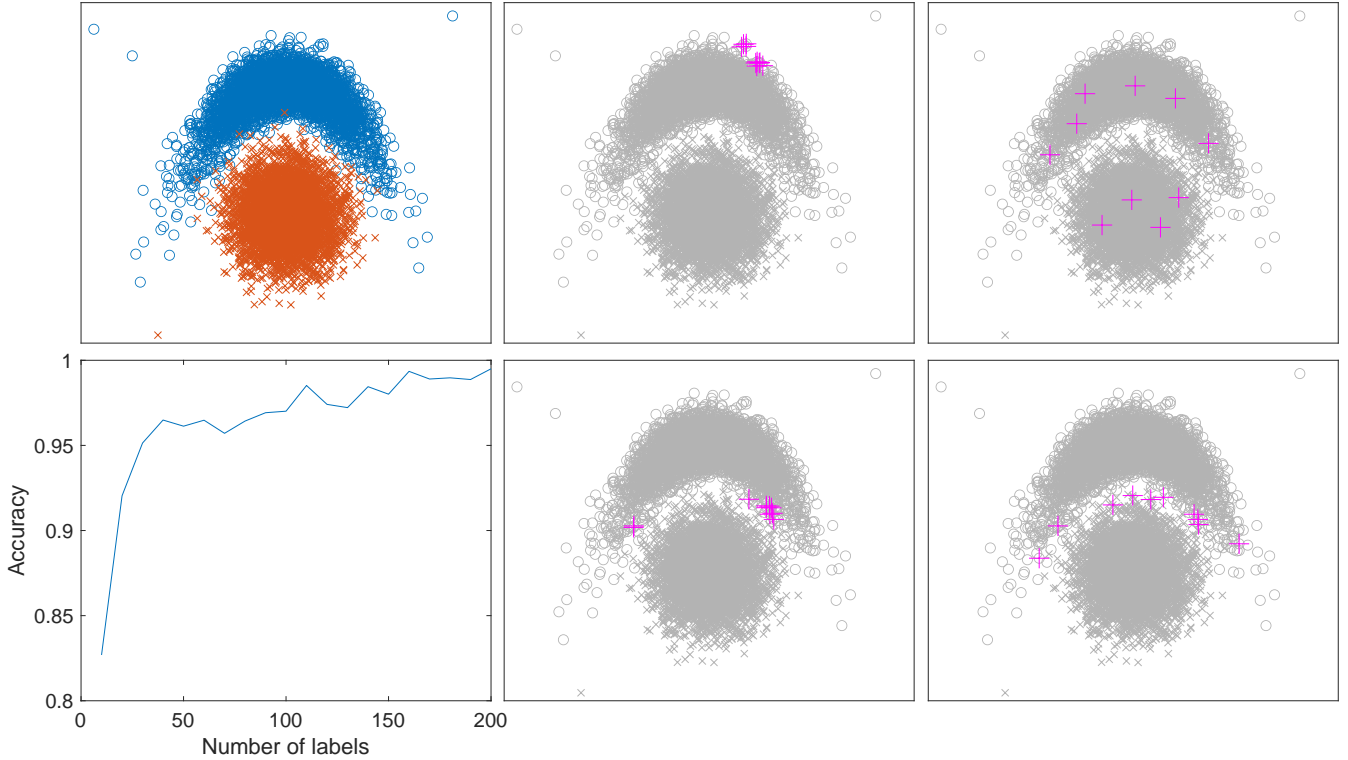


Figure 1: Our algorithm applied to an illustrative example. (Top left) A 2D binary classification problem: The dataset was sampled from a Gaussian distribution and a graph of cosine function with Gaussian noise. Few outliers are manually added. Two classes are highlighted with blue circles and orange x’s respectively. (Top right) The labels (magenta crosses) selected at the first 10 stages of active learning: Our algorithm selected u^1 which tends to sample distinct points within high-density areas. (Bottom right) The labels selected at the 51-th to 60-th stages. Here, our algorithm switched to u^2 and selected data points that lie close to the decision boundary formed by the learner. Note that outliers are not selected. (Middle) Simultaneously selecting data points with the highest entropy values leads to spatially aggregated labels. In particular, at early learning stages (Middle top), the entropy estimates of the learner f are inaccurate, leading to sampling uninformative points. (Bottom left) The classification accuracy of our algorithm with respect to the number of acquired labels.

0.5 times the average distances of data instances in X while the output kernel parameter σ_f is determined as the number of classes per dataset. The noise level σ^2 (Eq. 4) is kept at a small value 10^{-10} . These hyperparameters were determined without using the information of the problem or data at hand. In general, tuning them per task and dataset can improve the performance but this will require additional validation labels which might be hard to acquire in active learning (where labels are sparse). Sec. 4 demonstrates that the performance of our algorithm varies smoothly and predictably with respect to varying combinations of hyperparameter values.

The complexity of each iteration of our algorithm is $\mathcal{O}(K^2 \times N)$ with N and K being the number of (unlabeled) data instances and the sparse GP approximation rank (Eq. 5), respectively. For CIFAR10 dataset, on average our algorithm takes around 0.2 second to suggest a point to label. The corresponding run-times of *VAAL*, *CoreSet*, *LearningLoss*, *BADGE*, *WS*, *SeqGCN*, and *TA-VAAL* (See Sec. 4) were 23.73, 0.05, 0.12, 0.58, 0.03, 0.86, and 23.78 seconds respectively; While instantiating continuous learning, our approach incurs comparable computational costs.

4 Experiments

Settings: We assessed the performance of our algorithm on four benchmark datasets: The CIFAR10 dataset contains 60,000 color images of size 32×32 in 10 classes [Krizhevsky, 2009]. Among them, 50,000 images were used for training (5,000 images per class) while the remaining 10,000 images were reserved for testing. Similarly, the CIFAR100 dataset provides 60,000 images from 100 classes (500 images per class) [Krizhevsky, 2009]. The FashionMNIST [Xiao *et al.*, 2017] dataset consists of 70,000 28×28 grayscale images of 10 classes. Among them, 60,000 images were used for training while the remaining 10,000 images served as a test set. The Caltech256 dataset consists of 30,607 images from 256 object categories and a background class [Griffin *et al.*, 2007]. Here, the number of images per class and the size of each image vary. Total 22,897 and 7,710 images were used for training and testing, respectively.

For comparison, we also performed experiments with Sener and Savarese’s core-set approach (*CoreSet*) [Sener and Savarese, 2018], [Yoo and Kweon, 2019]’s learning loss (*LearningLoss*), [Sinha *et al.*, 2019]’s variational adversarial active learning (*VAAL*), [Kim *et al.*, 2021]’s task-aware

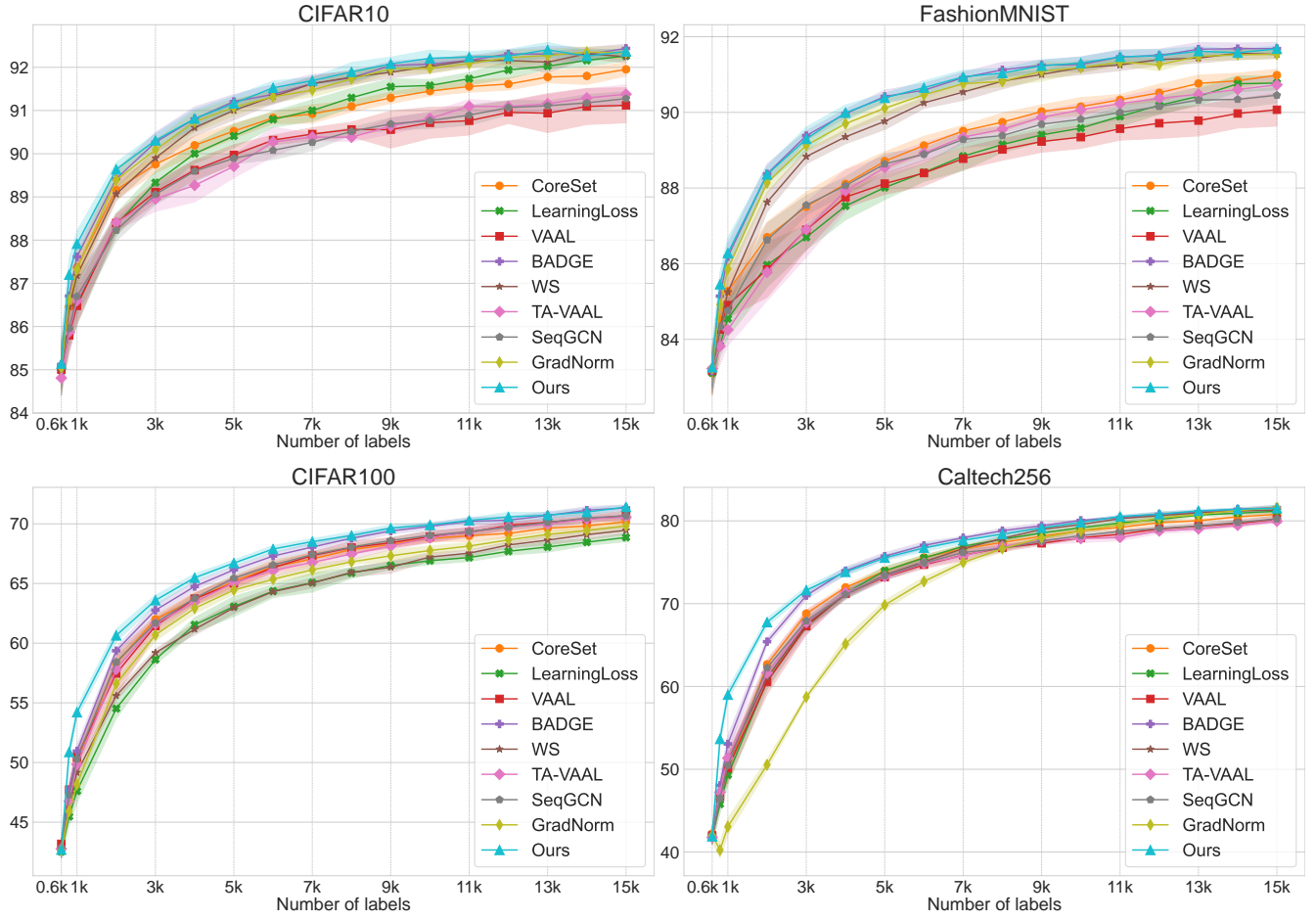


Figure 2: Accuracy (in %) of different active learning algorithms. The widths of the shaded regions represent twice the standard deviations.

VAAL-extension (*TA-VAAL*), [Caramalau *et al.*, 2021]’s sequential GCN-based algorithm (*SeqGCN*), [Ash *et al.*, 2020]’s batch active learning by diverse gradient embeddings (*BADGE*), [Wang *et al.*, 2022]’s gradient norm-based approach (*GradNorm*), and [Yun *et al.*, 2020]’s weight decay scheduling scheme (*WS*). Throughout the entire experiments, initially, 600 images were randomly labeled and the baseline learner was trained. Thereafter, the labels were augmented by the respective active learning algorithm until the label set met the final budget of $B = 15,000$. To assess the label acquisition performance at early learning stages, the learners were evaluated for 600, 800, and 1,000 labels, and thereafter they were evaluated at every 1,000 additional labels ($I=1,000$). This constitutes a set of experiments with varying labeling budgets $B = \{600, 800, 1000, \dots, 15,000\}$.

For the baseline learner of the active learning algorithms, we initially evaluated ResNet18 [He *et al.*, 2016], ResNet101 [He *et al.*, 2016], and VGG16 [Simonyan and Zisserman, 2015], all combined with fully connected (FC) layers matching the number of classes per dataset. Among them, we selected a ResNet101 pre-trained on ImageNet; Combining the *pool5* layer of ResNet101 with three FC layers consistently outperformed the other networks. Our learners were trained with stochastic gradient descent with an initial learn-

ing rate of 0.01. The learning rate was reduced to 10% for every 10 epochs. The mini-batch size and the total number of epochs were fixed at 30 and 100, respectively. For the GP surrogate \hat{f} , we used the *pool5* layer outputs of ResNet101 as inputs x . All experiments were repeated ten times with random initializations and the results were averaged. Our experiments were performed on a machine with Intel Core-i9 11900K CPU and Nvidia RTX3090 GPU.

Results: Figure 2 summarizes the results. As *CoreSet* and *VAAL* analyze the overall distribution of data, they are especially effective in detecting *influential* data points, achieving higher accuracies than other methods when labels are limited. However, exploration-based methods do not directly exploit the learner f ’s predictions, and consequently, they can fail to select *difficult* (or *uncertain*) data points. This led to degraded performances at later stages of learning where f provides more reliable uncertainty estimates. *WS*, *LearningLoss* and *BADGE* exploit this task-specific information achieving higher accuracies than *CoreSet* and *VAAL* at later learning stages of CIFAR10. *TA-VAAL* and *SeqGCN* yielded comparable performance to *VAAL*.

The performances of different algorithms varied significantly across datasets: CIFAR10 and FashionMNIST have

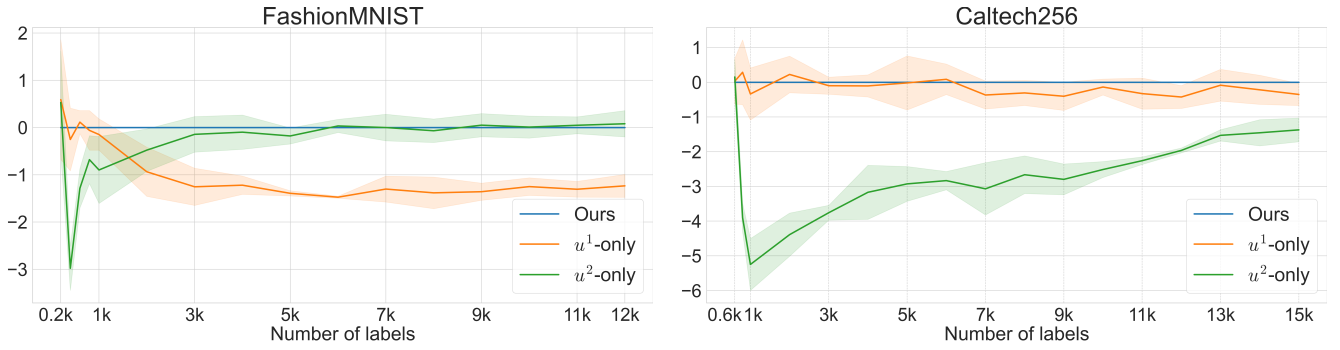


Figure 3: Performance of two variants of our final algorithm: u^1 -only and u^2 -only use only the u^1 and u^2 utilities, respectively. The y-axis represents the accuracy offset from our final algorithm. Negative offsets indicate that the final version is better. Our final algorithm offers an adequate trade-off between exploration and exploitation by combining the complementary strengths of u^1 and u^2 utilities.

only 10 classes. For them, even with small numbers of labels, the baseline learners provided highly accurate uncertainty predictions, and the exploitation-based methods *LearningLoss* and *WS* demonstrated superior performance. As CIFAR100 and Caltech256 have larger numbers of classes, even with large numbers of labels, the class predictions and uncertainty estimates of the learner f are unreliable. In this case, exploration-based methods (*VAAL* and *CoreSet*) showed higher accuracies (for CIFAR100 and Caltech256, respectively). By combining exploration and exploitation, *BADGE* obtained overall high accuracies than pure exploration- or exploitation-based methods. In particular, it achieved the best performance among the other baseline methods at early stages of FashionMNIST. Incorporating these two modes of active learning into a single Gaussian process model and thereby capturing the continuous learning behavior of f , our algorithm demonstrated further significant improvement on CIFAR100 and Caltech256. For CIFAR10 and FashionMNIST, our results are on par with the best algorithms compared (*WS* and *BADGE*). Note that for all algorithms evaluated in our experiments, the overall accuracies are much higher than the results reported in [Ash *et al.*, 2020; Sener and Savarese, 2018; Yoo and Kweon, 2019; Sinha *et al.*, 2019; Kim *et al.*, 2021] as we use stronger baseline learners.

Contributions of exploration and exploitation: We performed experiments with two variations of our final algorithm, which respectively use only u^1 (u^1 -only) and u^2 (u^2 -only). Figure 3 shows the results. Our exploration utility u^1 was more effective on CIFAR100 and at the early learning stages of FashionMNIST where the learner’s predictions are inaccurate. This performance advantage (over u^2 -only) disappeared at later learning stages of FashionMNIST as the baseline learner delivered more reliable confidence estimates. Our exploitation utility u^2 exhibited the opposite behavior. By combining their complementary strengths, thereby trading exploration and exploitation, our final algorithm consistently outperformed u^1 -only and u^2 -only.

Effect of varying hyperparameters: Our hyperparameters were fixed across datasets and they were determined without using the information of the problem or data at hand: In general, tuning them per task and dataset can improve the perfor-

mance but this will require additional validation labels which might be hard to acquire in active learning where labels are sparse.

On CIFAR10, increasing the number of basis points K (Eq. 5) slightly improved the performance until when it reaches 2,000 (up to around 0.06%, averaged on different numbers of labels) and the performance saturated there: Our choice of $K = 500$ was made based on the computational complexity (quadratic in K). The performance variation was negligible when the original σ_x value (Eq. 2) was magnified by a factor in the range of $[0.3, 8]$. However, the accuracy decreased rapidly when the magnification factors were less than 0.1. The effect of varying σ_y was similar (Eq. 2). The noise level σ^2 (Eq. 4) was kept at a small value 10^{-10} : varying this in the range of $\{10^{-8}, 10^{-9}, 10^{-11}, 10^{-12}\}$ did not show any noticeable performance variation. Increasing \mathcal{T} value by 2 led to moderate performance degradation (around -0.05%); Figure 4 shows the effect of varying σ_x , σ_y , and \mathcal{T} values.

5 Conclusions

We presented a new active learning algorithm that incorporates the exploration of the problem and exploitation of knowledge gained by the learners into a single Gaussian process (GP) model as a surrogate of the baseline neural network learner. For exploitation, our model offers an optimal label selection by maximizing the total gain of information per stage. During the exploitation, our computationally efficient GP surrogate is instantly updated each time a single label is provided, helping to faithfully simulate the continuous learning behavior of the baseline learner without actually having to retrain it. This enables to avoid having to introduce additional mechanisms to promote the label diversity which might require tuning separate hyperparameters. With experiments on four classification datasets with varying difficulty levels, we demonstrated that our algorithm significantly outperforms or is on par with the state-of-the-art.

Limitations and future work: Our two utility functions (respectively responsible for exploration and exploitation) offer theoretical rigor thanks to the use of the Bayesian framework. However, our approach to automatically deciding between these utilities is ad hoc and leaves room for improve-

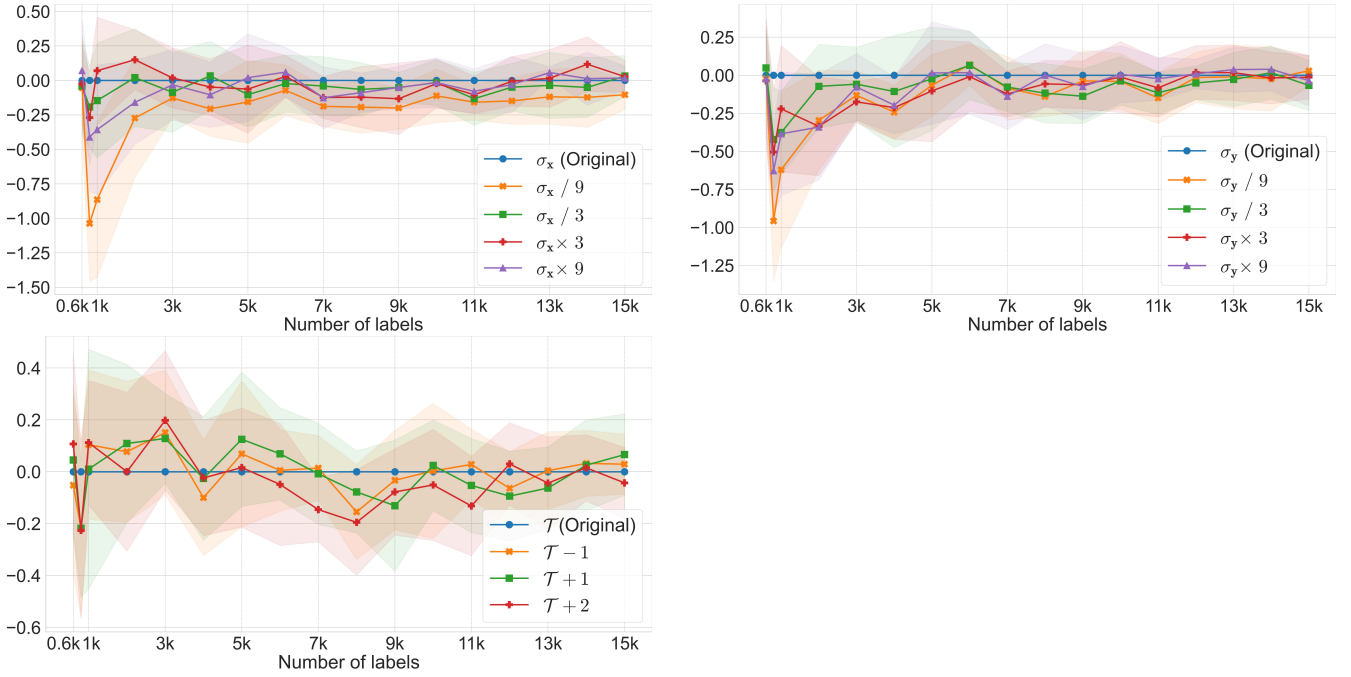


Figure 4: The effect of varying hyperparameter σ_x , σ_y , and \mathcal{T} values (CIFAR10 dataset; in raster order). The y-axis represents the accuracy offset from our final algorithm.

ment. Possible directions to address this include combining them with appropriately assigned weights or training a separate switching module that selects a suitable utility per data instance. Future work should explore these possibilities.

Our exploration-focused utility u^1 optimizes the information gain *per data instance*. However, unlike *CoreSet*, this greedy optimization strategy does not guarantee the *joint* optimality of all selected labels and therefore at the very early stages of CIFAR10, ours are only comparable to *CoreSet*. Future work should investigate extending our sequential selection scheme to joint optimization.

By construction, our GP surrogate \hat{f} is the same as f at every I -th stage, and in-between these stages, \hat{f} can deviate from f . Empirically, we observed that \hat{f} faithfully captures the behavior of f thanks to the product kernel k (Eq. 1) while a theoretical analysis of the quality of \hat{f} as a surrogate of f and its impact on the resulting active learning performance would help gain deeper insights into the utility of our algorithm. Future work should also explore this.

Acknowledgments

This work was supported by the National Research Foundation of Korea (NRF) grant (No. 2021R1A2C2012195), Institute of Information & Communications Technology Planning & Evaluation (IITP) grant (2021-0-00537, Visual Common Sense Through Self-supervised Learning for Restoration of Invisible Parts in Images), and IITP grant (2020-0-01336, Artificial Intelligence Graduate School Program, UNIST), all funded by the Korea government (MSIT).

References

- [Abu-El-Haija *et al.*, 2016] Sami Abu-El-Haija, Nisarg Kothari, Joonseok Lee, Paul Natsev, George Toderici, Balakrishnan Varadarajan, and Sudheendra Vijayanarasimhan. YouTube-8M: a large-scale video classification benchmark. In *arXiv:1609.08675*, 2016.
- [Aggarwal *et al.*, 2015] Charu C. Aggarwal, Xiangnan Kong, Quanquan Gu, Jiawei Han, and Philip S. Yu. Active learning: a survey. In Charu C. Aggarwal, editor, *Data Classification Algorithms and Applications*, pages 571–605. CRC Press, 2015.
- [Ailon, 2012] Nir Ailon. An active learning algorithm for ranking from pairwise preferences with an almost optimal query complexity. *JMLR*, 13:137–164, 2012.
- [Angeli *et al.*, 2021] Kevin De Angeli, Shang Gao, Mohammed Alawad, Hong-Jun Yoon, Noah Schaeferkoetter, Xiao-Cheng Wu, Eric B. Durbin, Jennifer Doherty, Antoinette Stroup, Linda Coyle, Lynne Penberthy, and Georgia Tourassi. Deep active learning for classifying cancer pathology reports. *BMC Bioinformatics*, 22:113:1–113:25, 2021.
- [Aodha *et al.*, 2014] Oisín Mac Aodha, Neill D. F. Campbell, Jan Kautz, and Gabriel J. Brostow. Hierarchical subquery evaluation for active learning on a graph. In *CVPR*, pages 564–571, 2014.
- [Ash *et al.*, 2020] Jordan T. Ash, Chicheng Zhang, Akshay Krishnamurthy, John Langford, and Alekh Agarwal. Deep batch active learning by diverse, uncertain gradient lower bounds. In *ICLR*, 2020.

- [Bodó *et al.*, 2011] Zalán Bodó, Zsolt Minier, and Lehel Csató. Active learning with clustering. In *Workshop on Active Learning and Experimental Design*, pages 127–139, 2011.
- [Bondu *et al.*, 2010] A. Bondu, V. Lemaire, and M. Boullé. Exploration vs. exploitation in active learning: a Bayesian approach. In *IJCNN*, 2010.
- [Budd *et al.*, 2019] Samuel Budd, Emma C. Robinson, and Bernhard Kainz. A survey on active learning and human-in-the-loop deep learning for medical image analysis. In *arXiv:1910.02923*, 2019.
- [Caramalau *et al.*, 2021] Razvan Caramalau, Binod Bhattarai, and Tae-Kyun Kim. Sequential graph convolutional network for active learning. In *CVPR*, pages 9583–9592, 2021.
- [Donmez and Carbonell, 2009] Pinar Donmez and Jaime G. Carbonell. Active sampling for rank learning via optimizing the area under the ROC curve. In *European Conference on Information Retrieval*, pages 78–89, 2009.
- [Elhamifar *et al.*, 2013] Ehsan Elhamifar, Guillermo Sapiro, Allen Yang, and S. Shankar Sastry. A convex optimization framework for active learning. In *ICCV*, pages 4321–4328, 2013.
- [Freytag *et al.*, 2014] Alexander Freytag, Erik Rodner, and Joachim Denzler. Selecting influential examples: active learning with expected model output changes. In *ECCV*, pages 562–577, 2014.
- [Geifman and El-Yaniv, 2017] Yonatan Geifman and Ran El-Yaniv. Deep active learning over the long tail. In *arXiv:1711.00941*, 2017.
- [Gissin and Shalev-Shwartz, 2019] Daniel Gissin and Shai Shalev-Shwartz. Discriminative active learning. In *arXiv:1907.06347*, 2019.
- [Griffin *et al.*, 2007] Greg Griffin, Alex Holub, and Pietro Perona. Caltech-256 object category dataset. Technical report, California Institute of Technology, 2007.
- [Guo, 2010] Yuhong Guo. Active instance sampling via matrix partition. In *NIPS*, pages 802–810, 2010.
- [He *et al.*, 2016] Kaiming He, Xiangyu Zhang, Shaoqing Ren, and Jian Sun. Deep residual learning for image recognition. In *CVPR*, pages 770–778, 2016.
- [Houlsby *et al.*, 2011] Neil Houlsby, Ferenc Huszár, Zoubin Ghahramani, and Máté Lengyel. Bayesian active learning for classification and preference learning. In *arXiv:1112.5745*, 2011.
- [Kim *et al.*, 2020] Taehun Kim, Kyunghwa Lee, Sungwon Ham, Beomhee Park, Sangwook Lee, Dayeong Hong, Guk Bae Kim, Yoon Soo Kyung, Choung-Soo Kim, and Namkug Kim. Active learning for accuracy enhancement of semantic segmentation with CNN-corrected label curations: Evaluation on kidney segmentation in abdominal CT. *Scientific Reports*, 10(366), 2020.
- [Kim *et al.*, 2021] Kwanyoung Kim, Dongwon Park, Kwang In Kim, and Se Young Chun. Task-aware variational adversarial active learning. In *CVPR*, pages 8166–8175, 2021.
- [Kirsch *et al.*, 2019] Andreas Kirsch, Joost van Amersfoort, and Yarin Gal. BatchBALD: efficient and diverse batch acquisition for deep Bayesian active learning. In *NeurIPS*, 2019.
- [Krizhevsky, 2009] Alex Krizhevsky. Learning multiple layers of features from tiny images. Technical report, University of Toronto, 2009.
- [Mohamed *et al.*, 2010] Thahir P. Mohamed, Jaime G. Carbonell, and Madhavi K. Ganapathiraju. Active learning for human protein-protein interaction prediction. *BMC Bioinformatics*, 11:1–9, 2010.
- [Rasmussen and Williams, 2006] Carl Edward Rasmussen and Christopher K. I. Williams. *Gaussian Processes for Machine Learning*. MIT Press, Cambridge, MA, 2006.
- [Ren *et al.*, 2020] Pengzhen Ren, Yun Xiao, Xiaojun Chang, Po-Yao Huang, Zhihui Li, Xiaojiang Chen, and Xin Wang. A survey of deep active learning. In *arXiv:2009.00236*, 2020.
- [Roy and McCallum, 2001] Nicholas Roy and Andrew McCallum. Toward optimal active learning through sampling estimation of error reduction. In *ICML*, pages 441–448, 2001.
- [Schott, 2016] James R. Schott. *Matrix Analysis for Statistics*. Wiley, New Jersey, 3rd edition, 2016.
- [Sener and Savarese, 2018] Ozan Sener and Silvio Savarese. Active learning for convolutional neural networks: a core-set approach. In *ICLR*, 2018.
- [Settles, 2009] Burr Settles. Active learning literature survey. Technical Report Computer Sciences Technical Report 1648, University of Wisconsin-Madison, 2009.
- [Siddhant and Lipton, 2018] Aditya Siddhant and Zachary C. Lipton. Deep Bayesian active learning for natural language processing: results of a large-scale empirical study. In *EMNLP*, pages 2904–2909, 2018.
- [Simonyan and Zisserman, 2015] K. Simonyan and A. Zisserman. Very deep convolutional networks for large-scale image recognition. In *ICLR*, page arXiv:1409.1556, 2015.
- [Sinha *et al.*, 2019] Samarth Sinha, Sayna Ebrahimi, and Trevor Darrell. Variational adversarial active learning. In *ICCV*, pages 5972–5981, 2019.
- [Smeulder, 2004] Hieu T. Nguyen Arnold Smeulder. Active learning using pre-clustering. In *ICML*, pages 623–630, 2004.
- [Snelson and Ghahramani, 2006] Edward Snelson and Zoubin Ghahramani. Sparse Gaussian processes using pseudo-inputs. In *NIPS*, 2006.
- [Sollich and Williams, 2005] Peter Sollich and Christopher K. I. Williams. Using the equivalent kernel to understand gaussian process regression. In *NIPS*, pages 1313–1320, 2005.

- [Tomanek and Hahn, 2009] Katrin Tomanek and Udo Hahn. Semi-supervised active learning for sequence labeling. In *EMNLP*, pages 1039–1047, 2009.
- [Tong and Koller, 2001] Simon Tong and Daphne Koller. Support vector machine active learning with applications to text classification. *JMLR*, 2:45–66, 2001.
- [Tran *et al.*, 2019] Toan Tran, Thanh-Toan Do, Ian Reid, and Gustavo Carneiro. Bayesian generative active deep learning. In *ICML*, pages 6295–6304, 2019.
- [Vijayanarasimhan and Kapoor, 2010] Sudheendra Vijayanarasimhan and Ashish Kapoor. Visual recognition and detection under bounded computational resources. In *CVPR*, pages 562–577, 2010.
- [Wang *et al.*, 2022] Tianyang Wang, Xingjian Li, Pengkun Yang, Guosheng Hu, Xiangrui Zeng, Siyu Huang, Cheng-Zhong Xu, and Min Xu. Boosting active learning via improving test performance. In *AAAI*, pages 8566–8574, 2022.
- [Xiao *et al.*, 2017] Han Xiao, Kashif Rasul, and Roland Vollgraf. FashionMNIST: a novel image dataset for benchmarking machine learning algorithms. In *arXiv:1708.07747*, 2017.
- [Yoo and Kweon, 2019] Donggeun Yoo and In So Kweon. Learning loss for active learning. In *CVPR*, pages 93–102, 2019.
- [Yun *et al.*, 2020] Juseung Yun, Byungjoo Kim, and Junmo Kim. Weight decay scheduling and knowledge distillation for active learning. In *ECCV*, pages 431–447, 2020.
- [Zhang *et al.*, 2020] Beichen Zhang, Liang Li, Shijie Yang, Shuhui Wang, Zheng-Jun Zha, and Qingming Huang. State-relabeling adversarial active learning. In *CVPR*, pages 8756–8765, 2020.